Adaptation and benchmarking of the pellet simulation code HPI2 for the stellarators TJ-II and W7-X

N. Panadero[1], K. J. McCarthy[1], J. Baldzuhn[2], E. de la Cal[1], F. Koechl[3], D. Iglesias[4], I. Pastor[1], J. L. Velasco[1], TJ-II team and W7-X team

[1]*Laboratorio Nacional de Fusión, CIEMAT, Madrid, Spain*
[2]*Max-Planck-Institut für Plasmaphysik, Greifswald, Germany*
[3]*Culham Centre for Fusion Energy, Culham Science Centre, Abingdon, UK*
[4]*Dept. Química Física Aplicada, Univ. Autónoma de Madrid, Madrid, Spain*

Cryogenic pellet injection (PI) is the best candidate for an efficient fuelling in large fusion devices, an issue of primary importance for the helical types [1]. Despite the important development of PI technologies and the advancement in the understanding of the involved physical phenomena, further effort is needed to achieve a deeper knowledge that allows optimizing the fuelling. In parallel, it is necessary to incorporate new insights into the underlying physics into simulation codes in order to improve predictions. For instance, the HIP2 code simulates the ablation of a cryogenic hydrogen pellet injected into a tokamak, as well as the evolution of the pellet plasmoid, using a 0D, two-cell, four-fluid Lagrangian system [2–4]. This code no only takes into account specific machine geometrical data, plasma energy and density profiles, but also the magnetic field configuration of the device. Later, in order to be used in helical devices, an extension, to include the effect of a helical field in the calculation of the drift acceleration force, was put in [5]. More recently, modifications to include a generalized calculation of the drift were added [6]. In this work, an overview of the adaptation and benchmarking of the HPI2 code [2–4] for the stellarators TJ-II and W7-X is presented. In addition, experiments dedicated to study the source of the differences between certain TJ-II experimental results and predictions [6, 7] are outlined. Indeed, the TJ-II PI database has been exploited to benchmark the new stellarator version of the HPI2 [6], allowing predictions for the W7-X. Firstly, these devices and their PI systems are described.

The TJ-II is a 4-period, low magnetic shear ($\Delta\iota \leq 6$ %) stellarator with a major radius R = 1.5 m, and an average minor radius $\langle a \rangle \leq 0.22$ m (plasma volume $V_{plasma} \sim 1.1$ m^3). Its magnetic-field, with bean shaped cross-section and central magnetic field, $B(0) \leq 1.1$ T, is created by a set of copper coils. Plasmas ($t_{discharge} \leq 300$ ms) are usually created and maintained using ECRH ($P \leq 500$ kW, $t \leq 300$ ms), achieving central electron densities, $n_e(0)$, of $\leq 1.7 \times 10^{19}$ m^{-3}, while electron and ion temperatures are $T_e(0) \leq 2$ keV and $T_i(0) \leq 120$ eV, respectively [8].

The TJ-II PI (see Figure 1a) is a 4-barrel pipe gun device with a cryogenic refrigerator for *in-situ* pellet formation (10 K), fast propellant valves for pellet acceleration ($v_p \sim$ 800-1200 m/s) and straight delivery lines. It is a flexible system, allowing injecting pellets of different sizes

from the low field side (LFS). These cylindrical pellets, from 0.42 mm to 1 mm in length and in diameter, contain between 3.1×10^{18} and 4.2×10^{19} H atoms. The PI is equipped with a light gate and a microwave cavity to estimate pellet velocity and mass [8]. Also, two amplified Si photodiodes, fitted with interference filters centred at 660 nm, follow the pellet cloud H_α emission (λ = 656.28 nm) from above (TOP) and behind (SIDE) pellet flight. In addition, a fast camera (FASTCAM APX-RS by Photron Inc.) records pellet injections from above (INNERTOP) or tangential (TANG) to the flight path. It is equipped with a coherent fibre bundle and a 12.5 mm lens. Its time resolution can be set, independently from the frame rate, from 1/frame rate to 1 μs, while the spatial resolution varies from 1024x1024 pixels to 16x128 pixels at maximum frame rate (250 kfps) (each pixel corresponds to ~0.5 mm to ~1 mm along the pellet flight path, depending on the viewport). Recently, to allow recording simultaneously from both viewports, and hence determining the 3D pellet trajectory, the system has been upgraded by substituting the fibre bundle with a double bundle (Figure 1b).

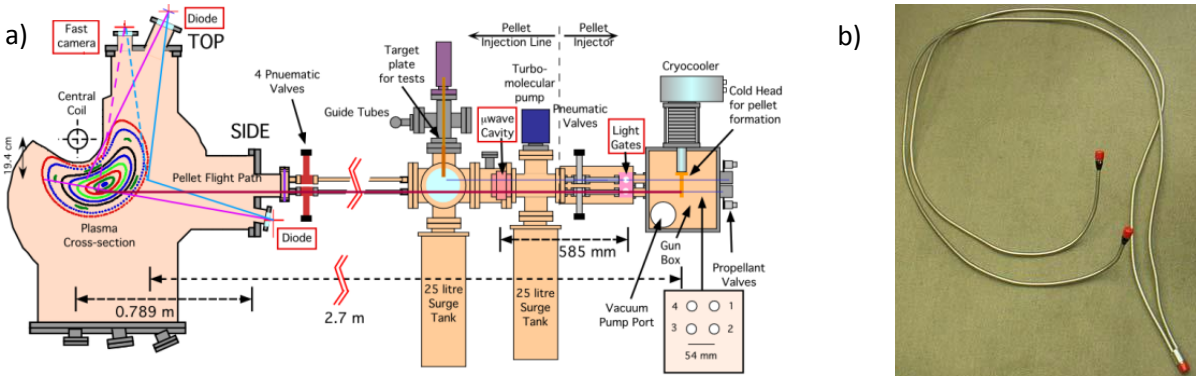

Figure 1. a) Cross-sectional sketch of the TJ-II vacuum chamber, magnetic surfaces, and the pellet injector. The relative locations of pellet Lines#1 through #4 are indicated with respect to the rear of the PI. b) Photography of the 4.5 m long double- bundle. Each branch is 6 mm x 6 mm, with a fibre density of 45 lines/mm.

The optimized stellarator Wendelstein 7-X has a R = 5.5 m and an $\langle a \rangle$ = 0.55 m ($V_{plasma} \sim 30$ m^3). Its optimized magnetic field is generated by a set of 70 superconducting NbTi coils (B(0) ≤3 T). ECRH is its main heating system, formed by 10 gyrotrons (P ≤8 MW, t ≤30 min) [9].

The ASDEX-U blower-gun injector [10] is currently installed on W7-X, allowing injections from both the LFS and the High Field Side (HFS) of the device at $v_{pellet} \sim$ 170–230 m/s ($f_{pellet} \sim$ 2–30 Hz). These cylindrical hydrogen pellets, with nominal size of 2 mm in diameter and in length, contain ≤ 3.3×10^{18} atoms [11]. Each injection line is equipped with a microwave cavity to measure pellet mass and velocity. Also, a fast PIN-photodiode collects the pellet cloud light. In addition, a set of standard and fast cameras is able to record pellets from different directions and with different temporal and spatial resolutions [11].

As mentioned, the HPI2 has been extended to non-axisymmetric devices by including an average calculation of magnetic and geometric quantities in the determination of the plasmoid drift. This is done by using the equilibrium magnetic configuration to evaluate these quantities, averaged along plasmoid parallel length [6]. Predictions obtained with this approach have been compared to TJ-II experimental results. Good agreement is found in general, except when suprathermal electrons are present in the plasma core [6]. In this situation, a significantly higher fuelling efficiency (FE) is observed [7]. Simulations that include the effect of suprathermal electrons in the pellet ablation have been also carried out (see Figure 2), with a significant number of assumptions related to the suprathermal electron energies and distributions (pitch angles are neglected). However, even with these simplifications, the predicted ablation profile is significantly modified and closer to the measured H_α. However, density evolution and FE are still not reproduced by the HPI2. It has been proposed that suprathermal electrons affect plasmoid expansion, modifying the drift [7]

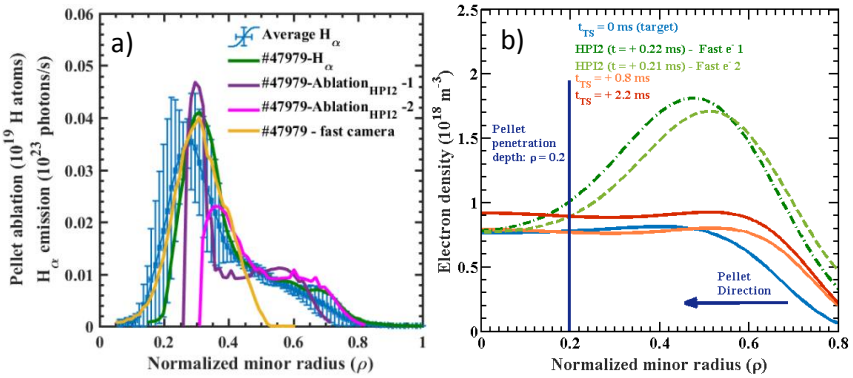

Figure 2. a) HPI2 ablation (purple and magenta) profiles compared with measured H_α profile (green) for a pellet injected along Line-1 into an off-axis ECRH plasma (discharge #47979, $5.5x10^{18}$ H atoms, v_p = 959.7 m/s). Also, average H_α emission (blue) is shown. In addition, the light profile obtained from the montage of snap-shots images (yellow) from fast camera is plotted. b) TS electron density profiles measured before (blue) and after injection (orange and brick red) plus HPI2 (dark and olive green) predicted density profiles.

Regarding W7-X, given the good agreement with TJ-II experiments (except when suprathermal electrons are present), HPI2 predictions are expected to be reliable. Therefore, a set of simulations was carried out as a preliminary study for the experimental campaign OP 1.2, comparing LFS and HFS injections with for two plasma scenarios (high density and high temperature). It was predicted that, as observed in tokamaks, material deposition is deeper and FE is higher for HFS injections. Also, it was obtained that lower plasma temperatures increase pellet penetration and plasmoid drift [6]. Afterwards, using OP 1.2 data is input, first comparisons between HPI2 predictions and experimental results have been done. For instance, in Figure 3, predictions for LFS and HFS injections are compared. Similar pellet penetrations and FEs are obtained for both cases, consistent with experimental values [11]. However, the deeper deposition predicted for the HFS case is not observed [11].

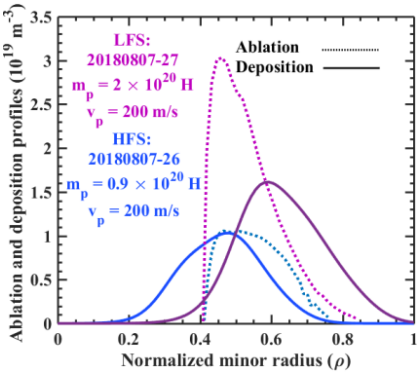

Figure 3. HPI2 ablation (dotted lines) and deposition (solid lines) profiles for pellets injected into W7-X experiments 20180807-27 (purple, 2 x10^{20} H atoms, v_p = 200 m/s) and 20180808-26 (blue, 0.9x10^{20} H atoms).

Finally, in order to understand the disagreement when PIs are made into plasmas with suprathermal electrons, a series of experiments has been performed in TJ-II. As observed in Figure 4, where the radial drift as a function of the pellet position is plotted for a series of discharges with different populations of suprathermal electrons, the drift seems to be reduced when suprathermal electrons are present. In some cases, even detached plasmoids, drifting inwards, are observed. However, it should be noted that it is not possible to determine the poloidal drift, and hence, the double-bundle should be used. Unfortunately, the number of PI made using this improved set-up is still reduced and no conclusions can be extracted.

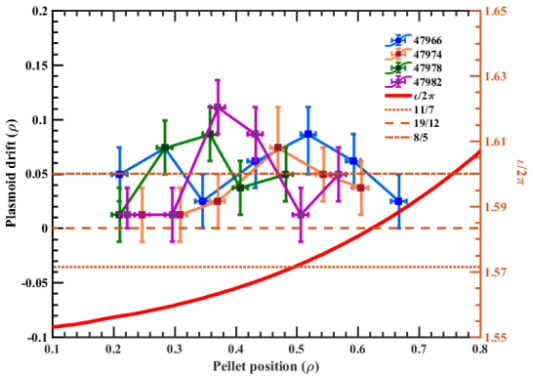

Figure 4. Plasmoid radial drift as a function of pellet position for different discharges, recorded from INNER TOP viewport (75 kfps, τ_{exp} = 1 μs). Suprathermal population increases with discharge number (#47966 does not have). On the right axis, ι-profile (red) and relevant low order rational surfaces (brick red) are indicated.

"This work has been carried out within the framework of the EUROfusion Consortium and has received funding from the Euratom research and training programme 2014-2018 and 2019-2020 under grant agreement No 633053. The views and opinions expressed herein do not necessarily reflect those of the European Commission."

[1] H. Maaßberg, C.D. Beidler, E.E. Simmet, *Plasma Phys. Control. Fusion* **41** (1999) 1135–1153.
[2] B. Pégourié *et al.*, *Plasma Phys. Control. Fusion* **47** (2005) 17–35.
[3] B. Pegourie *et al.*, *Nucl. Fusion* **47** (2007) 44–56.
[4] F. Köchl *et al.*, *Prepr. EFDA–JET–PR(12)57* (2012) 82.
[5] A. Matsuyama *et al.*, *Nucl. Fusion* **52** (2012) 123017.
[6] N. Panadero *et al.*, *Nucl. Fusion* **58** (2018) 026025.
[7] K.J. McCarthy *et al.*, *Plasma Phys. Control. Fusion* **61** (2019) 014013.
[8] E. Ascasibar *et al.*, *Nucl. Fusion* (2019) *accepted.*
[9] S.K. Combs *et al.*, *Fusion Sci. Technol.* **64** (2013) 513–520.
[10] T. Klinger *et al.*, *Nucl. Fusion* **59** (2019) 112004.
[11] M. Dibon *et al.*, *Fusion Eng. Des.* **98–99** (2015) 1759–1762.
[12] J. Baldzuhn *et al.*, *Plasma Phys. Control. Fusion* (2019) (under consideration).